10th IMC
10th International Masonry Conference
G. Milani, A. Taliercio and S. Garrity (eds.)
Milan, Italy, July 9-11, 2018

INCREASE IN SEISMIC RESISTANCE FOR A DRY JOINT MASONRY ARCH SUBJECTED TO HINGE CONTROL

Gabriel L. Stockdale[1], Vasilis Sarhosis[2], and Gabriele Milani[1]

[1] Dept. of Architecture, Built Environment and Construction Engineering, Politecnico di Milano
Piazza Leonardo da Vinci 32, 20133 Milan, Italy
{gabriellee.stockdale, gabriele.milani}@polimi.it

[2] School of Engineering and Geosciences, Newcastle University
Newcastle upon Tyne, NE1 7RU, UK
e-mail: vasilis.sarhosis@newcastle.ac.uk

[1] Dept. of Architecture, Built Environment and Construction Engineering, Politecnico di Milano
Piazza Leonardo da Vinci 32, 20133 Milan, Italy
e-mail: gabriele.milani@polimi.it

Keywords: Masonry Arch, Tilt Test, Mechanization Optimization, Hinge Control, .

Abstract. *Damages to vaulted masonry and their vulnerability to seismic activities are continuously observed with each new earthquake. The behaviour of these systems is becoming well understood, and reinforcement strategies and techniques are continually advancing. It is often the case however that the application of reinforcement is done in such a manner that the failure of the system is transformed directly from one of stability to strength. This direct transformation overlooks the intermittent stages that exist between stability and strength, and thus provides an incomplete picture to the potential behaviours of the system. With the objective of maintaining the four-hinged mechanization failure, this work experimentally examines the increase in resistance that occurs through controlling the available positions for hinge development of a dry-stack masonry arch subjected to constant horizontal accelerations. From this experimentation, it is observed that controlling the hinge locations can increase the resistance of the arch while also providing a defined failure mechanism.*

1 INTRODUCTION

The assessment of existing structural systems is a necessary and important component in the management of a society's infrastructure. Especially after a natural disaster, such as an earthquake, the ability to perform efficient and effective structural assessments is critical. This criticality of efficiency is even further exacerbated when considering elements of cultural heritage where there is often a significant lack of funding for even routine maintenance, and the structure itself is of little economic importance towards the functionality of the society [1]. In these circumstances, as well as others, the development of tools to aid in the efficient assessment of structural systems can play a significant role in maximizing preservation efforts.

For structural masonry, and specifically masonry arches this criticality of assessment not only exists for the preservation of cultural heritage, but also for the management of civil structures still in operation. Between the United Kingdom, Italy and Spain there are over 52,000 masonry arch bridges in active use today [2-5]. There does exist a significant amount of analysis techniques and strategies, and experimental investigations aimed at the assessment of arches and existing structures [2,6-7]. These techniques and their appropriate applications provide a solid framework for establishing a reliable and comprehensive understanding of most arch conditions analysed, but the labour and computational costs can be very high. The challenge at this point is not in the ability to analyse an arch, but in efficiently determining which arches require a more in-depth analysis and which ones can be accepted in their post disaster state as is or with minor adjustments. To meet this challenge, first order assessment strategies need to be developed.

Recently, the idea was introduced to look beyond the limiting mechanism of the masonry arch and consider the behaviour of the mechanism itself and the role it can have on the system if it were changed [8]. Initial investigations into this idea through the use of FE analysis have been performed [9,10]. These investigations have shown that the arch can be strengthened, and the mechanism can be defined. Therefore, the next stage is to begin the experimental investigation into this controlled mechanization behaviour.

This work presents the development and execution of an experimental campaign aimed at gaining an insight into the relationship between admissible mechanisms and structural capacity for an arch. With the objective of controlling the four-hinged mechanization failure of a dry joint masonry arch, the constant horizontal acceleration capacity of the arch was measured through a tilt table. First, an equilibrium approach to the upper-bound theorem of limit analysis that is utilized for both the experimental setup and analysis of results is presented in section 2. Section 3 describes the experimental setup and is followed by the procedure in section 4. Section 5 presents the data. The initial results are then discussed in section 6, and lastly some concluding remarks in section 7.

2 LIMIT ANALYSIS

Limit analysis is considered the most reliable tool for the analysis of masonry arches [6,11]. Using the rigid no tension model and the assumption of no slippage between blocks, the upper bound theorem of limit analysis provides the ideal starting point for an experimental analysis structure [12]. The upper bound theorem, or the kinematic approach, states that an arch will only collapse if there exists a kinematically admissible mechanism that produces zero or positive work. For the constant horizontal acceleration condition a kinematically admissible mechanism requires four hinges that alternate between the intrados and extrados of the arch as shown in figure 1. From the mechanism in figure 1, it can be seen that the mechanical arch can be represented as three rigid elements connected by pins as seen in figure 2.

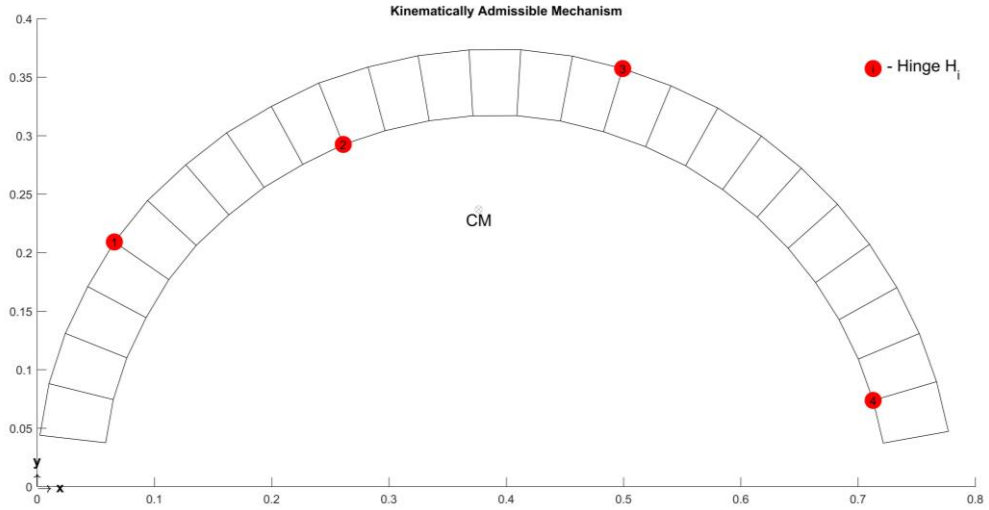

Figure 1: Example of a kinematically admissible mechanism for a masonry arch.

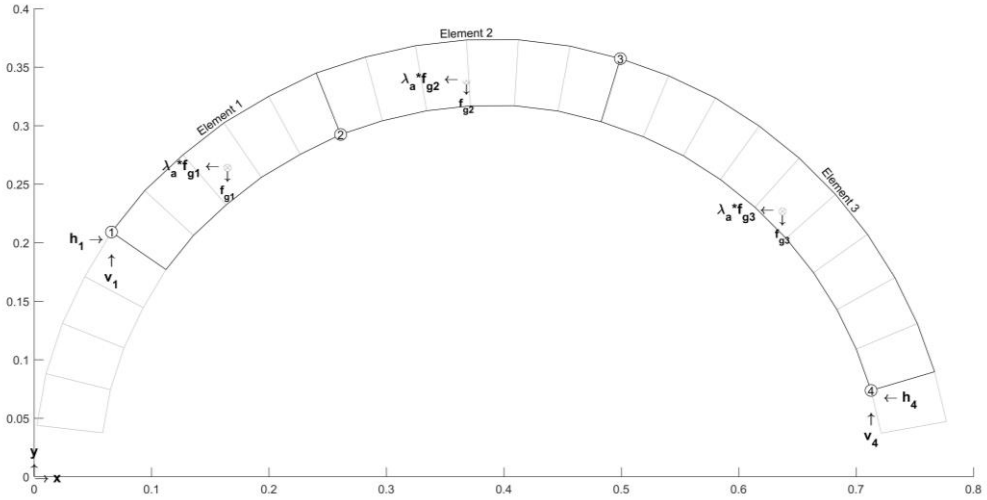

Figure 2: Equilibrium condition for a mechanized hinge represented by three rigid elements connected by four perfect hinges subjected to a constant horizontal acceleration.

The equilibrium conditions for the system in figure 2, reveals nine equations and eight unknowns, but the inclusion of the force developed by the horizontal acceleration as a reaction produces a determinate system. This determinate system then allows for the direct calculation of both the collapse condition, and hinge reactions through solving the set of equilibrium equations. The constant horizontal acceleration loading condition shown in figure 2 can be decomposed into the three elements. Assuming perfect hinges and summing the moments of elements one, two and three at the same numbered hinges respectively produces the equilibrium equations

$$\begin{bmatrix} -1 & 0 & 1 & 0 & 0 & 0 & 0 & 0 & f_{g1} \\ 0 & 1 & 0 & -1 & 0 & 0 & 0 & 0 & 0 \\ 0 & 0 & -\Delta y_{2,1} & \Delta x_{1,2} & 0 & 0 & 0 & 0 & -f_{g1}\Delta y_{CM1,1} \\ 0 & 0 & -1 & 0 & 1 & 0 & 0 & 0 & f_{g2} \\ 0 & 0 & 0 & 1 & 0 & 1 & 0 & 0 & 0 \\ 0 & 0 & 0 & 0 & \Delta y_{3,2} & \Delta x_{2,3} & 0 & 0 & f_{g2}\Delta y_{2,CM2} \\ 0 & 0 & 0 & 0 & -1 & 0 & 1 & 0 & f_{g3} \\ 0 & 0 & 0 & 0 & 0 & -1 & 0 & 1 & 0 \\ 0 & 0 & 0 & 0 & 0 & 0 & \Delta y_{3,4} & -\Delta x_{3,4} & f_{g3}\Delta y_{3,CM3} \end{bmatrix} \begin{bmatrix} h_1 \\ v_1 \\ h_2 \\ v_2 \\ h_3 \\ v_3 \\ h_4 \\ v_4 \\ \lambda_a \end{bmatrix} = \begin{bmatrix} 0 \\ f_{g1} \\ -f_{g1}\Delta x_{1,CM1} \\ 0 \\ f_{g2} \\ f_{g2}\Delta x_{2,CM2} \\ 0 \\ f_{g3} \\ -f_{g3}\Delta x_{3,CM3} \end{bmatrix} \quad (1)$$

shown in matrix form. The hinge reactions and collapse load for a given kinematically admissible hinge set can then be determined through simple matrix manipulations.

3 EXPERIMENTAL SETUP

A 27-block semi-circular arch was chosen for this experimentation. From previous computational analyses it is clear that when either base hinge, hinge H_1 or H_4 (see figure 1), vertically exceed the centre of mass of the full arch, the assumption of no slippage no longer holds [9,10]. With the two base blocks fixed to the support, the 27 block arch results in an allowed variation of five joints for both hinges H_1 and H_4, and ultimately 25 distinct minimum mechanisms.

3.1 Arch construction

The arch was constructed with timber blocks. Timber was chosen as the block material to ensure the blocks could endure a minimum of 75 collapses to measure the 25 mechanisms. Each arch block was constructed from three 47mm x 75mm Canadian Lumber Standard timber boards. First, both 75mm sides of one board and one 75mm side on each other boards were planed. The planed sides were glued together and then each face of the combined boards was planed to produce clean faces with sharp edges. The purpose of combining the three boards was to increase the depth and create a more stable arch with respect to the out-of-plane behaviour. Finally, a trapezoid template was constructed with a short span of 38mm and tapered sides of 3.33° from square. This template was used to mark and cut each block.

After each block was cut, its faces that make the arch boundary joints were scarified to increase roughness. The blocks were then assembled and adjusted to establish the most stable configuration (see figure 3**)**. Next, they were numbered and oriented, and the exposed faces were painted white. Finally, a four by four grid of fixed distance points was established across each joint with the template also shown in figure 3. The mass, dimensions and point grid lengths of each block were measured and recorded.

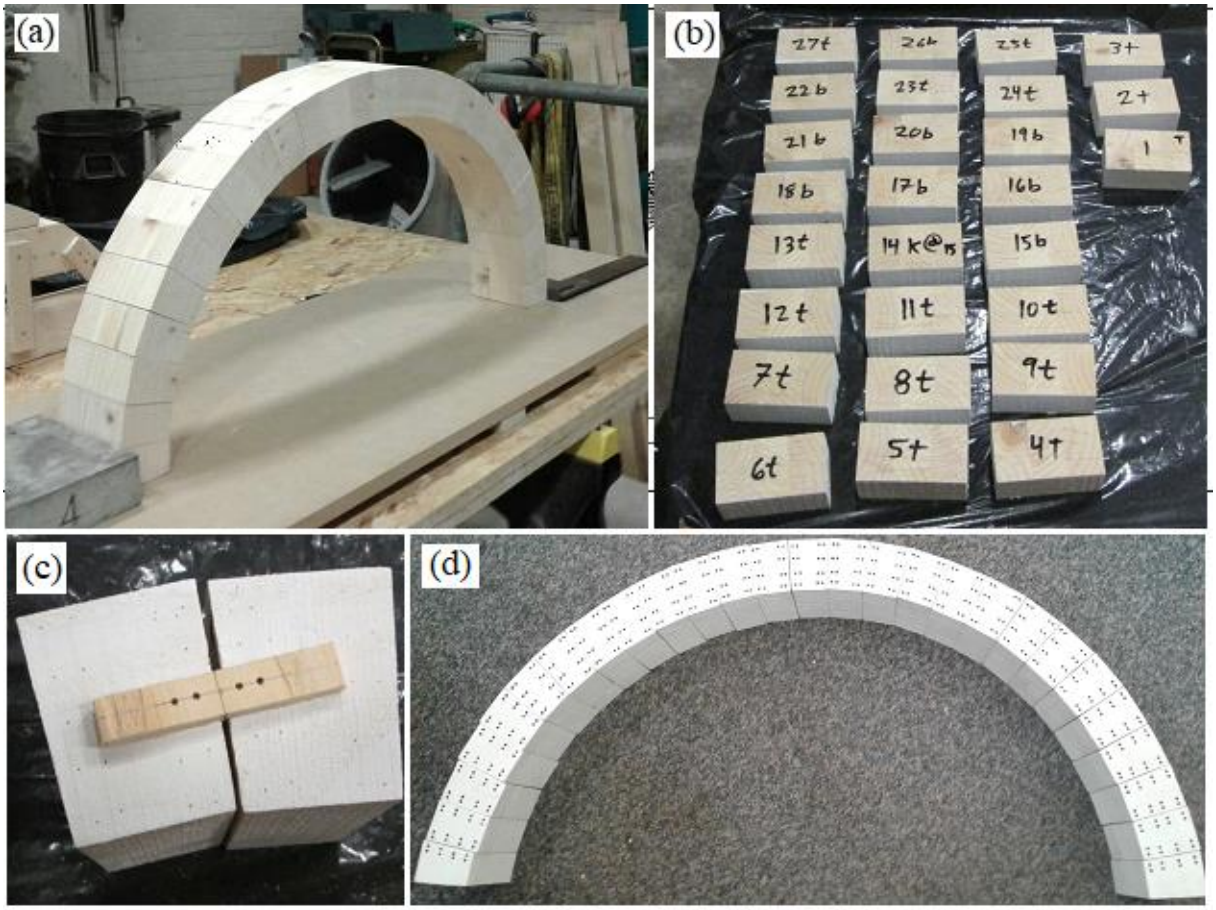

Figure 3: Photographs of (a) the best fit block configuration; the (b) bock and orientation marking; the (c) the parallel point joint grid template; and (d) the final assembled arch.

Figure 4 shows the final constructed arch and the platform. The base blocks were set from left to right. The left base was anchored to the platform by screws anchored underneath the platform. The arch was assembled, shims were added to the extrados of the right base block to provide the most stable configuration prior to anchoring it to the platform. The final arch has a clear span of 0.6695±0.0005 m and a rise of 0.3170±0.0005 m. The platform was made from a dense composite board with risers to allow the use of the negative space for anchoring. The riser on the left in figure 4 was placed with a straight edge running the width of the platform and perpendicular to the arch to ensure in-plane rotations. A threaded steel bar was attached parallel to the rotation edge and a lifting chain was attached to the bar at the centreline of the arch plane. Nuts and washers were added to the threaded bar to remove potential out of plane motions.

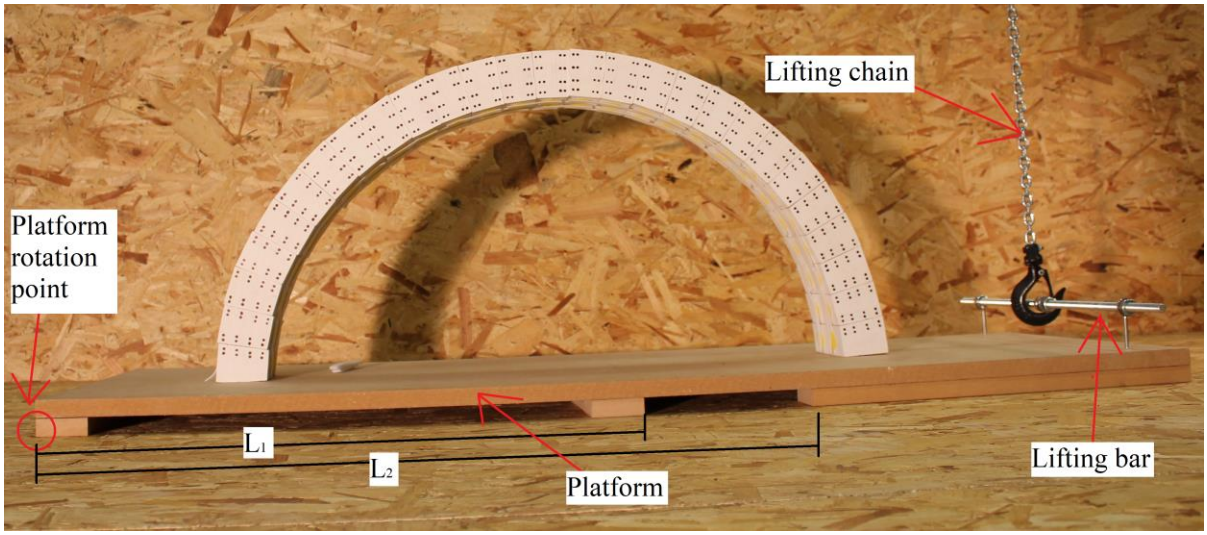

Figure 4: Image and annotation of the experimental setup. L_1 and L_2 are marked and measured lengths along the plane of the platform.

3.2 Hinge control

The final component of the arch construction is the hinge control system. The hinge control system was constructed with Velcro®. The light weight of the timber blocks allows the use of the shear strength of Velcro® to resist hinge rotations while its lighter weight ensures a negligible effect to the stable system. Two circular hook-sided tabs were adhered on both the intrados and extrados of each block such that tabs align in two parallel planes when the arch is standing as can be seen in figure 5. Hinge control was then achieved through applying loop-sided straps across all but the hinge joints which can also be seen in figure 5.

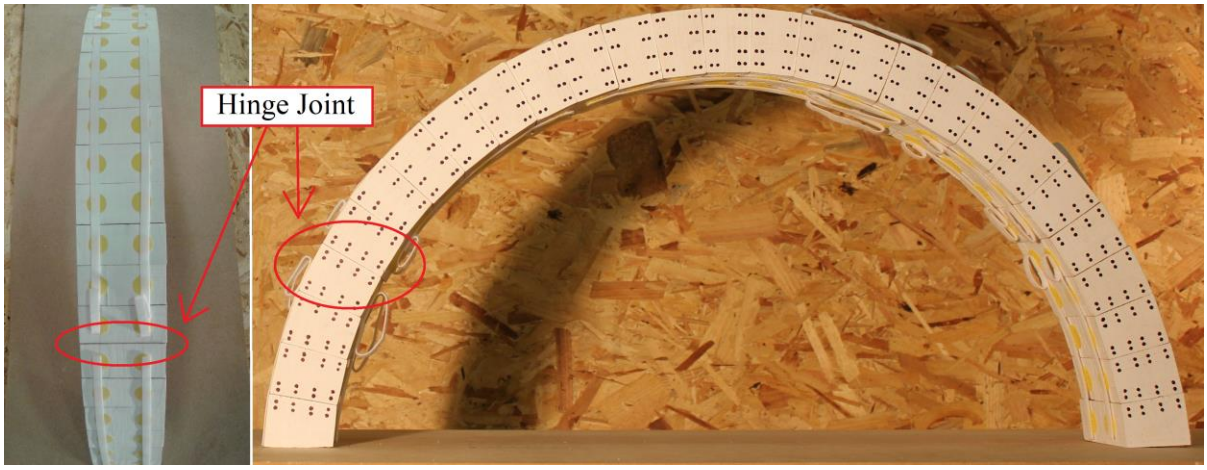

Figure 5: Photos highlighting the location of a defined hinge joint through the Velcro$^{\theta}$ reinforcement.

3.3 Arch analysis model

The arch analysis model was constructed in AutoCAD®. Due to the high sensitivity that is associated with the block angels at the scale of the arch constructed, a statistical approach was taken to constructing the model. For example of this sensitivity, the difference between a 27 block and 23 block arch with a thickness of 54 mm is a 0.5 mm change in either the intrados or extrados. Therefore, the dimensions of the blocks were averaged. The averaged block dimensions are shown in figure 6. The averaged block was drawn in AutoCAD® and the arch

was constructed starting from the left base block. Next, the intrados and extrados of random blocks were altered within the precision of the averaged blocks until the arch fit the clear span, rise, and slight rotation observed in the right base block. A lidar scan of the arch face was also taken. The 2D face of the drawn arch was compared against the point cloud from the scan. As can be seen in figure 6, the two results are in good agreement. Finally, the boundary points, area and centroid of each block in the drawn arch was recorded. Figure 7 shows the final drawn arch and the nomenclature used in the Procedure, Data, Results and Conclusion sections of this work.

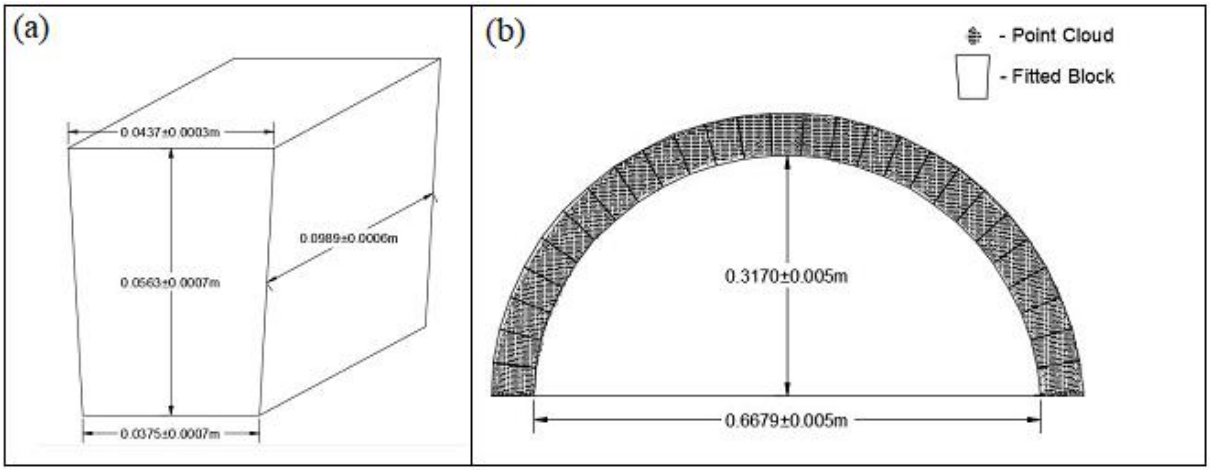

Figure 6: (a) The dimensions of the averaged block used for the analysis model, and (b) the comparison of the fitted arch developed from the averaged block and the recorded point cloud of the built arch.

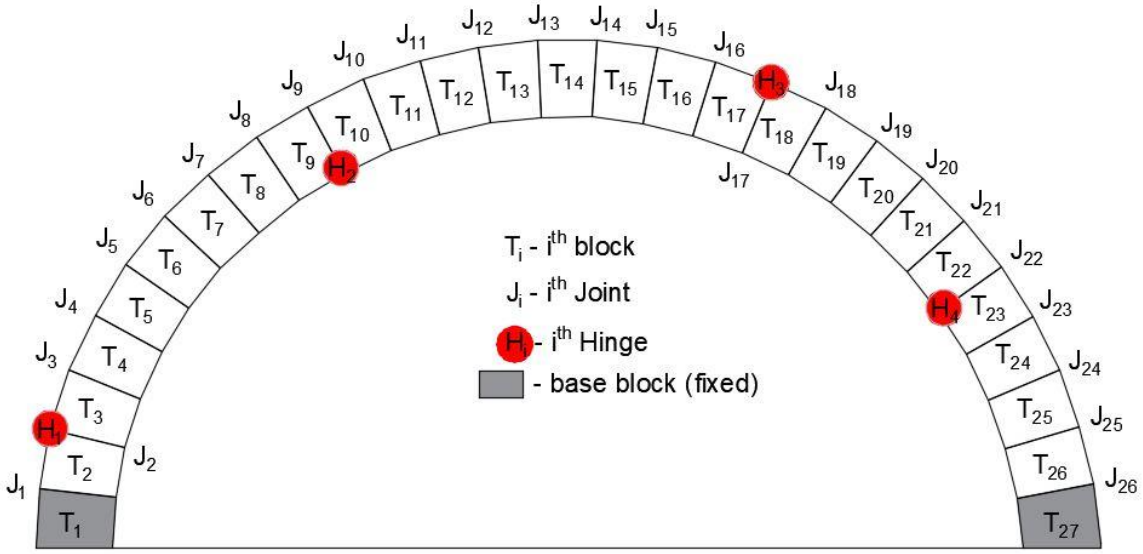

Figure 7: Defined nomenclature for the experimental arch.

3.4 Tilt Table

The tilt table method was utilized to introduce quasi-static horizontal accelerations [13]. Gravity's constant direction and magnitude result in the rotation of acceleration being equal to the tilting plane's rotation. Therefore, a rotation of the tilting plane of θ_t, is equivalent to applying a horizontal acceleration of magnitude $\lambda_a \cdot g$ with

$$\lambda_a = \tan(\theta_t) \tag{2}$$

and

$$\theta_t = \sin^{-1}\frac{l}{L} \tag{3}$$

where l is the measured height after rotation of a known distance L along the plane of the board (see figure 4).

4 PROCEDURE

The procedure for this experimental program consisted of assembling the arch, applying the Velcro® loop straps to set the hinge locations, tilting the table until collapse and measuring the resulting heights l_1 and l_2 corresponding to known lengths L_1 and L_2 respectively (see figure 8).

4.1 Hinge Selection

As previously stated, this experiment examined 25 defined hinge configurations. The hinge configurations were developed by setting the base hinges (i.e. hinges H_1 and H_4) and performing a minimum operation on equation 1 applied to all the possible configurations for hinges H_2 and H_3 of an ideal semi-circular arch. The hinge configurations are listed in table 1.

Hinge Set	H_1	H_2	H_3	H_4	Hinge Set	H_1	H_2	H_3	H_4
1	J_1	J_8	J_{17}	J_{26}	**16**	J_4	J_{10}	J_{18}	J_{22}
2	J_1	J_8	J_{17}	J_{25}	**17**	J_4	J_{10}	J_{19}	J_{23}
3	J_1	J_8	J_{16}	J_{24}	**18**	J_4	J_{10}	J_{19}	J_{24}
4	J_1	J_8	J_{16}	J_{23}	**19**	J_4	J_{11}	J_{19}	J_{25}
5	J_1	J_8	J_{16}	J_{22}	**20**	J_4	J_{11}	J_{19}	J_{26}
6	J_2	J_8	J_{17}	J_{22}	**21**	J_5	J_{12}	J_{20}	J_{26}
7	J_2	J_9	J_{17}	J_{23}	**22**	J_5	J_{11}	J_{20}	J_{25}
8	J_2	J_9	J_{17}	J_{24}	**23**	J_5	J_{11}	J_{20}	J_{24}
9	J_2	J_9	J_{17}	J_{25}	**24**	J_5	J_{11}	J_{19}	J_{23}
10	J_2	J_9	J_{18}	J_{26}	**25**	J_5	J_{11}	J_{19}	J_{22}
11	J_3	J_{10}	J_{18}	J_{26}	Note: Refer to figure 7 for identifying joint location.				
12	J_3	J_{10}	J_{18}	J_{25}					
13	J_3	J_{10}	J_{17}	J_{24}					
14	J_3	J_9	J_{17}	J_{23}					
15	J_3	J_9	J_{18}	J_{22}					

Table 1: Defined hinge configurations for each measured hinge set.

The Velcro® loop straps were adjusted after each collapse to remove any plastic deformations that develop from the shock of collapse between the hook and loop interface of the Velcro®.

4.2 Collapse and Measurements

For each hinge set, a minimum of three collapses were performed. For each collapse the platform was rotated manually by raising the lifting chain with a reverse locking hand crank causing the platform to pivot about the rotation point (see figure 8). The chain was raised until

the arch collapsed and at a rate that maintained a quasi-static acceleration state. At the point of collapse the crank was locked and the heights l_1 and l_2 were recorded. The platform was then lowered, and the system was reassembled. Each collapse was also recorded with a Cannon DSLR camera.

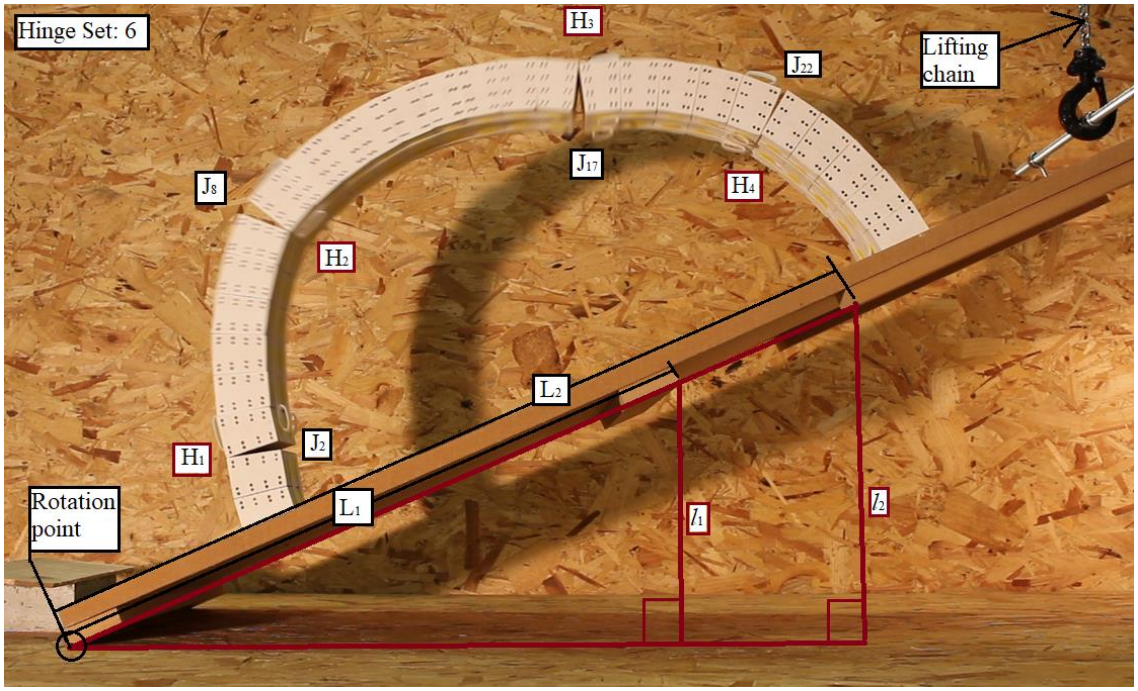

Figure 8: The mechanical collapse of the experimental arch and accompanying annotation of the defined (black) and measured (red) characteristics. H_i and J_i represent the i^{th} hinge and joint respectively. L_1 and L_2 are the known platform lengths and l_1 and l_2 are the measured heights at collapse.

5 DATA

The platform lengths L_1 and L_2 were measured at 0.6110±0.0005 m and 0.7880±0.0005 m respectively. For each collapse, the heights and observed failure methods were recorded. The recorded values and observations are presented in table A1 of Appendix A.

6 RESULTS

This work presents a first order assessment of the measured results by comparing the sets of collapse multipliers obtained through experimentation with those obtained through limit analysis.

6.1 Experimental Results

The calculated collapse multipliers were obtained by first averaging the ratio of the height to platform length measurements for each run. Equations 2 and 3 were then employed to obtain the collapse multiplier (λ_a) for each run. The average and standard deviation of λ_a was then calculated for each hinge set. The measurement error was manually propagated due to the simplicity of the performed calculations and variables. Finally, the propagated measurement error was compared against the standard deviation to establish the precision and identify its source. The resulting collapse load multipliers, precision and the source of the controlling error are presented in table 2.

Hinge Set	λ_a	±	source	Hinge Set	λ_a	±	source
1	0.32	0.02	stdv	**16**	0.67	0.01	stdv
2	0.32	0.02	stdv	**17**	0.60	0.01	stdv
3	0.323	0.008	stdv	**18**	0.56	0.05	stdv
4	0.32	0.04	stdv	**19**	0.54	0.03	stdv
5	0.31	0.01	stdv	**20**	0.519	0.003	meas
6	0.43	0.02	stdv	**21**	0.623	0.004	meas
7	0.42	0.02	stdv	**22**	0.62	0.04	stdv
8	0.42	0.02	stdv	**23**	0.67	0.04	stdv
9	0.423	0.004	stdv	**24**	0.65	0.02	stdv
10	0.398	0.006	stdv	**25**	0.72	0.03	stdv
11	0.45	0.04	stdv	* meas – measurement error stdv – standard deviation Note: Refer to table 1 for identifying hinge sets.			
12	0.48	0.02	stdv				
13	0.50	0.01	stdv				
14	0.523	0.006	stdv				
15	0.53	0.02	stdv				

Table 2: Calculated collapse multiplier, precision and controlling error source for each hinge set.

To better observe the results and overall behaviour of the arch, a collapse diagram was constructed by plotting the collapse multiplier against the negative tangent of the angle between hinges H_1 and H_4. Next, lines are drawn for all values of H_1 and H_4 connecting the points associated with the fixed base hinge value. The point of rotation for the tangent calculation was taken as the location where the centre of mass of the full arch (obtained from the arch model) crosses through the horizontal axis. Figure 9 shows the resulting load diagram from the results in table 2.

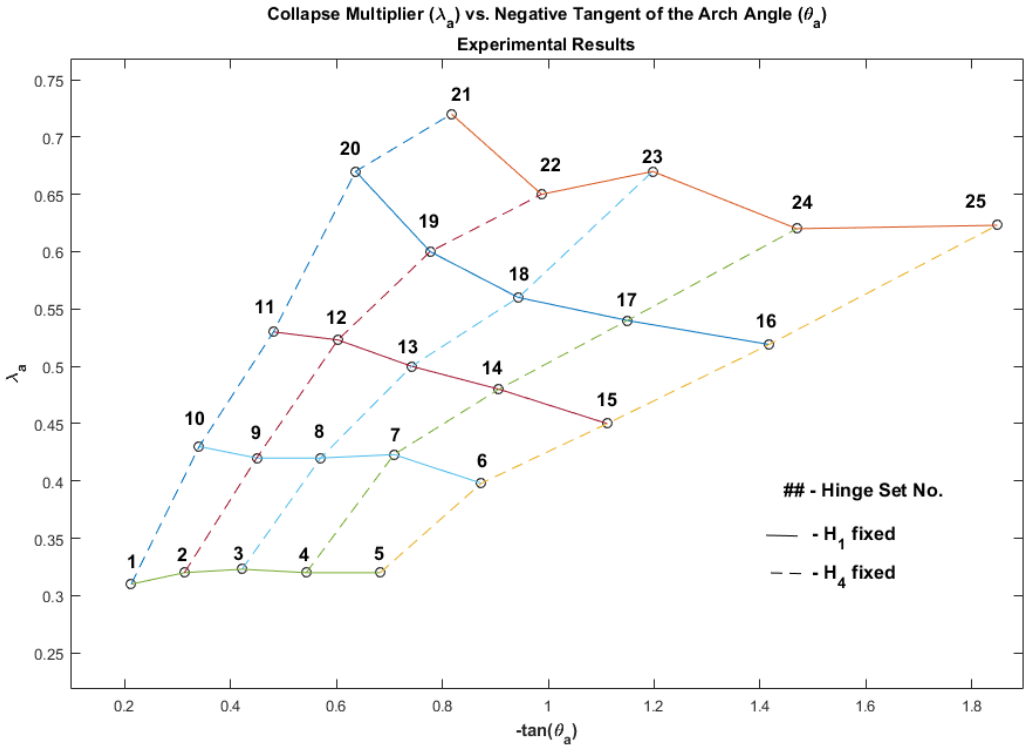

Figure 9: Plot of the collapse multipliers (λ_a) obtained experimentally against the negative tangent of the arch angles (θ_a).

6.2 Limit Analysis Results

Utilizing equation 1, the geometry properties of the modelled arch and the measured mass of each block, the same collapse diagram was developed for the limit analysis model. The diagram is shown in figure 10.

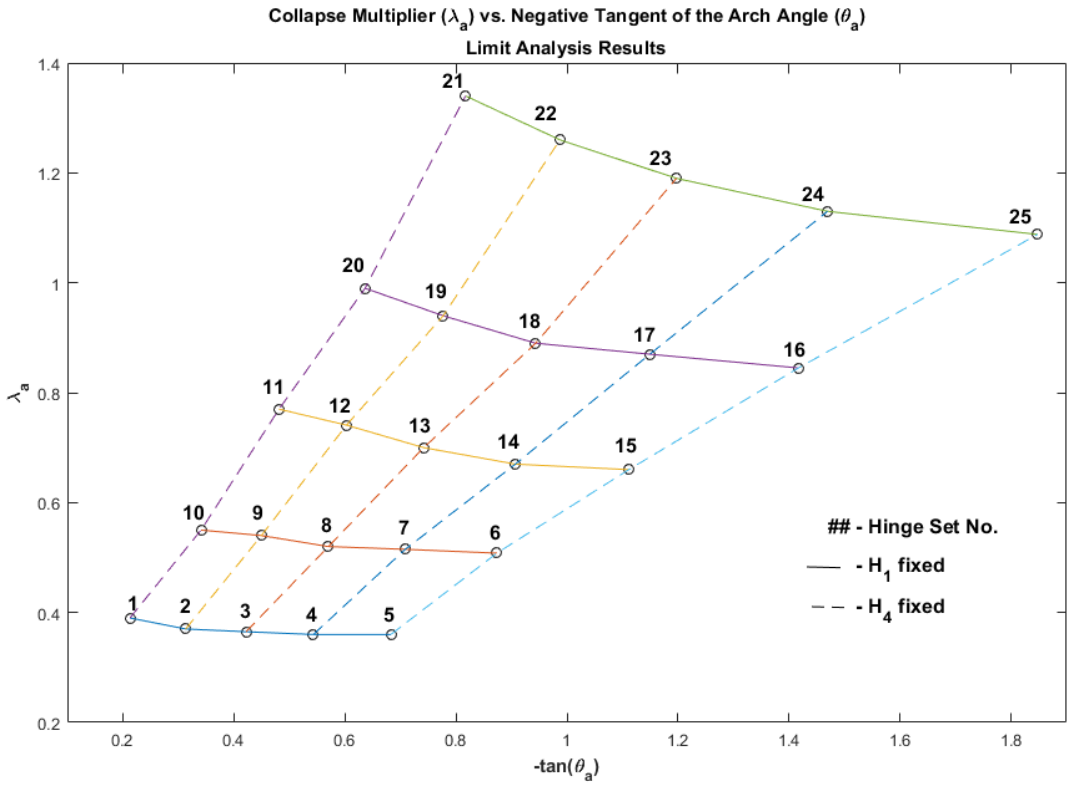

Figure 10: Plot of the collapse multipliers (λ_a) obtained through the limit analysis against the negative tangent of the arch angles (θ_a).

6.3 Comparison of Results

Figure 11 shows the overlay of the experimental and limit analysis results as well as a plot of the ratio between the experimental and limit analysis results. From figure 11a, it is clear that the behaviour of the mechanized arch was captured, but the capacity of the experimentation was significantly less than the values obtained through the limit analysis. Note also that the capacity of the arch is dominated by the location of hinge H_1. In figure 11b, it can be seen that there is relatively constant values for each fixed H_1 collapse set.

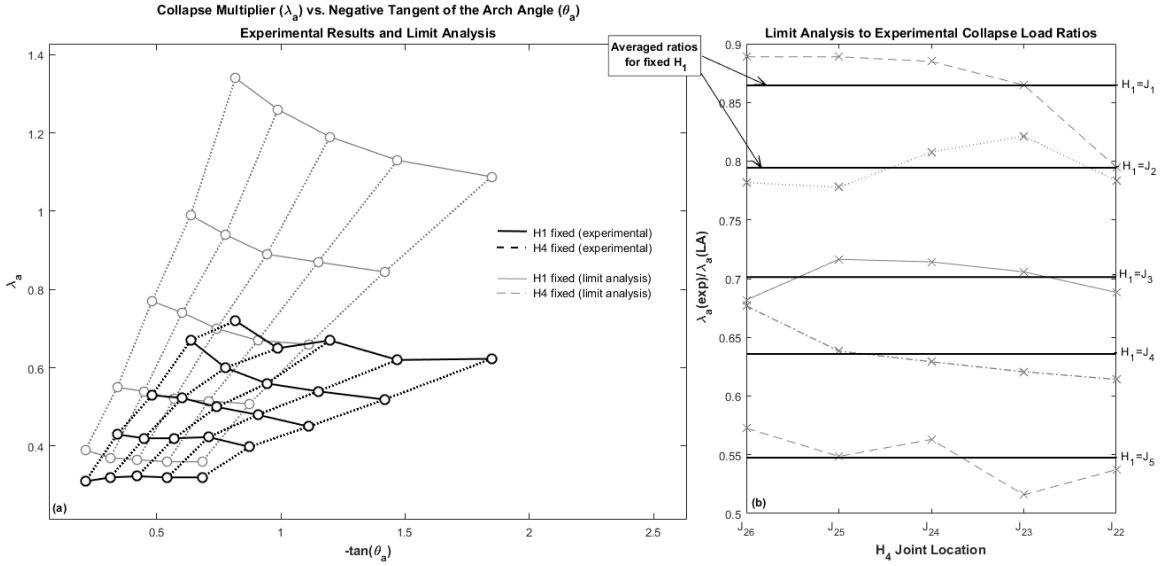

Figure 11: (a) Comparison of the experimental and limit analysis results for the collapse multipliers (λ_a) plotted against the negative tangent of the arch angles (θ_a), and (b) plots of the ratios between the experimental and limit analysis results for fixed hinge H_1 sets.

Between the comparison of the limit analysis and experimental analysis collapse results and ratio values, and in conjunction with the precision of the measured data it can be stipulated that there is at least one systematic error in the applied limit analysis approach.

7 CONCLUSIONS

The assessment of existing structural systems is a necessary and important component in the management of a society's infrastructure. The development of tools to aid in the efficient assessment of structural systems can play a significant role in maximizing preservation efforts. For structural masonry first order assessment strategies need to be developed, and any developed technique requires experimental testing. This work presents such experimental testing. Aimed at gaining an insight into the relationship between admissible mechanisms and structural capacity for an arch, controlled four-hinged mechanization failures of a dry joint masonry arch were examined for the constant horizontal acceleration collapse condition. From this experiment and its initial analysis, it appears that the arch's behaviour is controlled by the mechanisation failure, but there exists some systematic error in the limit analysis model that must be investigated.

7.1 Next Steps

As previously mentioned, each collapse was recorded. These recordings will be examined in detail, and in combination with the block joint grids will be utilized to develop an optical hinge rotation measurement system. From these resulting observations the cause of the apparent systematic error will be examined.

8 APPENDIX A: RECORDED DATA

Platform Measurements		precision	* M - MACHANISM
L1 [mm]	L2 [mm]	+/- 0.5 mm	S - SLIP
611	788		R - ROTATION

COLLAPSE DATA

Run	Hinge Set	l1 [mm]	l2 [mm]	Failure type *	notes:
1	1	172	222	M	
2	1	190	247.5	M	
3	1	187	245	MS	SMALL S AT H1
4	1	188	245.5	M	
11	1	187	245	M	
5	2	187	245	M	
6	2	194	248	M	
7	2	174	227	MS	SMALL S AT H1
8	2	195	254	M	
9	2	174.5	227	M	
10	2	189	246	MS	MODERATE S AT H1
12	3	190	247	MS	MODERATE S AT H1
13	3	191	248	MS	MODERATE S AT H1
14	3	184	239.5	M	
15	3	183	238	M	
16	4	178.5	232.5	M	
17	4	203	295	MS	SMALL S AT H1
18	4	174	227	MSM	MECH-SLIP-MECH
19	4	181	235.5	M	
20	5	187	244	MS	VERY SMALL S AT H1
21	5	177	230	M	
22	5	182	238.5	MSM	MECH-SLIP-MECH
23	6	230	298.5	M	
24	6	246	320	MR	SMALL OUT OF PLANE ROTATION
25	6	243	313.5	M	GOOD M
26	7	228	295	M	
27	7	243	313.5	M	
28	7	237	307.5	M	
29	8	233	302	M	ALLIGNMENT LITTLE OFF AT H1
30	8	243.5	312	M	
31	8	228	295	M	
32	9	238.5	309.5	M	GOOD M AND DOT ALLIGNMENT
33	9	237.5	309	M	
34	9	235	305.5	M	ALLIGNMENT LITTLE OFF AT H1 AND H3
35	10	222.5	289	M	ALLIGNMENT OFF AT H1
36	10	228	296	M	ALLIGNMENT OFF AT H1 AND H2
37	10	225.5	293	SM	S AT H1 M BEGINS AT HALF BLOCK THICKNESS
38	11	248	322	M	
39	11	271	351	MRS	SMALL S AND R AT H1 THEN M
40	11	233	303	MS	SMALL S AT H1 FROM FIXED SECTION
41	12	256	334	MS	SMALL SLIP/SHIFT AT H1
42	12	259	336	M	
43	12	275	355.5	M	SMALL STATIC TWIST AT H3 AT START
44	13	264	341.5	MS	VERY SMALL S AT H1
45	13	275	356	MS	VERY SMALL S AT H1
46	13	275	356	SM	SMALL S AT H1 THEN M
47	14	281	364	SM	SMALL S AT H1 THEN M
48	14	281	364	SM	SMALL S AT H1 THEN M
49	14	285.5	369	SM	SMALL S AT H1 THEN M
50	15	292	377.5	SM	SMALL S AT H1 THEN M
51	15	283	366.5	SM	SMALL S AT H1 THEN M
52	15	279	362	SM	SMALL S AT H1 THEN M
53	16	346	447	MS	VERY SMALL S AT H1
54	16	337	436.5	MS	VERY SMALL S AT H1
55	16	337	435	MS	VERY SMALL S AT H1
56	17	315.5	409	SM	SMALL S AT H1 THEN M
57	17	315	407.5	SM	SMALL S AT H1 THEN M S AT H1 M BEGINS AT 1/2 BLOCK THICKNESS
58	17	307	398	SM	BLOCK THICKNESS
59	18	301	392	SM	SMALL S AT H1 THEN M S AT H1 M BEGINS AT 1/2
60	18	314	416	SM	BLOCK THICKNESS S AT H1 M BEGINS AT 1/2
61	18	275	355	SM	BLOCK THICKNESS S AT H1 M BEGINS AT 1/2
62	19	296	383.5	SM	BLOCK THICKNESS S AT H1 M BEGINS AT 1/2
63	19	300	388.5	SM	BLOCK THICKNESS S AT H1 M BEGINS AT 1/2
64	19	273	355	SM	BLOCK THICKNESS S AT H1 M BEGINS AT 1/2
65	20	280	363.5	SM	BLOCK THICKNESS S AT H1 M BEGINS AT 1/2
66	20	279	363	SM	BLOCK THICKNESS S AT H1 M BEGINS AT 1/2
67	20	282	365.5	SM	BLOCK THICKNESS
68	21	321.5	417	M	SOME ROTATIONS AT J=1 RESTRAINED
69	21	322	418	M	SOME ROTATIONS AT J=1 RESTRAINED
70	21	323	419	M	SOME ROTATIONS AT J=1 RESTRAINED
71	22	339.5	439	M	LESS ROT AT J=1
72	22	314	406	M	LESS ROT AT J=1
73	22	313	404	M	LESS ROT AT J=2
74	23	324.5	423	M	LESS ROT AT J=2
75	23	351	454	M	LESS ROT AT J=2
76	23	343.5	442	M	LESS ROT AT J=2
77	24	336.5	435.5	M	LESS ROT AT J=1
78	24	326.5	422.5	M	SOME ROTATIONS AT J=1 RESTRAINED
79	24	339	439	M	SOME ROTATIONS AT J=1 RESTRAINED
80	25	364	469	MSR	H4 SLIDE-ROTATE, H1 SLIDE-ROTATE SOME TWIST
81	25	343	445	MSR	H4 SLIDE-ROTATE, H1 SLIDE-ROTATE SOME TWIST
82	25	363	468.5	MSR	H4 SLIDE-ROTATE, H1 SLIDE-ROTATE SOME TWIST

Table A1: Measurements, observed failure, and order of each recorded collapse.

REFERENCES

[1] G. Smith, *B, Disaster Recovery Funding: Achieving a Resilient Future?* Committee on Post-Disaster Recovery of a Community's Public Health, Medical, and Social Services; Board on Health Sciences Policy; Institute of Medicine. Healthy, Resilient, and Sustainable Communities After Disasters: Strategies, Opportunities, and Planning for Recovery. National Academies Press: Washington, DC, 2015

[2] V. Sarhosis, S. De Santis, G. di Felice, A review of experimental investigations and assessment methods for masonry arch bridges. *Structure and Infrastructure Engineering*, **12**(11): 1439-1464, 2016.

[3] J. Page, *Masonry arch bridges. State of art review*. Department of Transport, Transport Research Laboratory, London: HMSO, 1993.

[4] S. De Santis, G. de Felice, Overview of railway masonry bridges with a safety factor estimate. *International Journal of Architectural Heritage*, **8**(3) 452-474, 2014.

[5] J.A. Martin-Caro, *Puentes de Fabrica. Los puentes ferroviarios dentro del patrimonio industrial [Fabrica bridges. The railway bridges within the industrial heritage]*. Madrid: ADIF 2013 (in Spanish)

[6] A. Tralli, C. Alassandri, G. Milani, Computational methods for masonry vaults: a review of recent results. *Open Journal of Civil Engineering*, **8**(1): 272-287, 2014

[7] A.W. Hendry, *Structural Masonry*. Macmillan: Palgrave Macmillan, 1998.

[8] G. Stockdale, Reinforced stability-based design: a theoretical introduction through a mechanically reinforced masonry arch. *International Journal of Masonry Research and Innovation*, **1**(2): 101-142, 2016.

[9] G. Stockdale, G. Milani (2017) FE Model Predicting the Load Carrying Capacity of Progressive FRP Strengthening of Masonry Arches Subjected to Settlement Damage. *Key Engineering Materials*, **747**(1) 128-133, 2017.

[10] G. Stockdale, G Milani,(2017) FE model predicting the increase in seismic resistance induced by the progressive FRP strengthening on already damaged masonry arches subjected to settlement. *Int. Conference of Computational Methods in Sciences and Engineering*. AIP Conference Proceedings **1096**, 090002, Thessaloniki, Greece, 2017.

[11] J. Heyman, The stone skeleton. *International Journal of Solids and Structures*, **2**(2), 249-279, 1966.

[12] M. Angelillo (ed), *Mechanics of Masonry Structures*. Springer: London, 2014.

[13] M. DeJong, *Seismic Assessment Strategies for Masonry Structures*, PhD Dissertation, Massachusetts Institute of Technology, Massachusetts, 2009.